JOURNAL OF GEOPHYSICAL RESEARCH, VOL. 114, C03012, doi:10.1029/2008JC004793, 2009

Upper mixed layer temperature and salinity variability in the tropical boundary of the California Current, 1997–2007

Jose Gomez-Valdes[1] and Gilberto Jeronimo[1,2]

Received 6 March 2008; revised 17 October 2008; accepted 12 January 2009; published 17 March 2009.

[1] Spatial and temporal interannual variability of mixed layer (ML) temperature and ML salinity off Baja California are examined using empirical orthogonal functions analysis. Conductivity-temperature-depth data collected from October 1997 through January 2007 over a grid based on Mexican Research of the California Current quarterly survey cruises are analyzed. Net heat flux (NHF) and sea surface height anomaly (SSH) from satellite products are also analyzed. The first leading mode of both ML temperature and ML salinity show a single-signed loading pattern, in which the variability increases southward. Those patterns have been reported before, but they are lacking a quantitative explanation. ML temperature variability is mainly associated with NHF variability, while ML salinity variability is mainly associated with large-scale SSH variability. The principal component (PC) of ML salinity is correlated with North Pacific Gyre Oscillation and Warm Water Volume climate indices, while the PC of ML temperature is only correlated with the latter index. Those results indicate that the principal mode of ML salinity variability is a diagnostic variable of basin-scale process. An abrupt freshening (~ -0.7) and cooling ($\sim -4^{\circ}$C) event from January 1998 to January 1999 and an abrupt freshening (~ -0.5) event from January 2002 to January 2003 are conspicuous features in the mixed layer. The 1998–1999 events are associated with the major El Niño–La Niña cycle in the 10-year period. The 2002–2003 freshening is related to an enhancement of subarctic water into the equatorward flow that started during the summer of 2002 off Oregon (49°N).

Citation: Gomez-Valdes, J., and G. Jeronimo (2009), Upper mixed layer temperature and salinity variability in the tropical boundary of the California Current, 1997–2007, *J. Geophys. Res.*, *114*, C03012, doi:10.1029/2008JC004793.

1. Introduction

[2] The exchange of momentum, heat, and mass between the ocean and the atmosphere are widely known sources of variability at different timescales of temperature and salinity in the open upper ocean. In particular, in the Pacific Ocean the major sources of variability at interannual and decadal timescales are the large-scale climate modes such as El Niño–Southern Oscillation (ENSO) and the Pacific Decadal Oscillation (PDO) [*Miller*, 1996; *Doney et al.*, 2007]. In the California Current System, local wind patterns are also sources of low-frequency variability [*Auad et al.*, 1991; *Miller et al.*, 2004], rendering the prediction of mixed layer (ML) properties a more difficult task. For example, using California Cooperative Oceanic Fisheries (CalCOFI) data files for 1950 through 1962, *Lynn* [1967] found that between 35°N and 21°N the variability of temperature and salinity at 10 m depth is higher in the southern portion of that region. He suggested that it is due to large nonseasonal variations of these properties as compared with their seasonal changes. *Jeronimo and Gomez-Valdes* [2006] found the same pattern off Baja California (32–24°N) using the mean temperature and salinity distributions on the 25 σ_θ isopycnal calculated from the Mexican Research of the California Current (IMECOCAL) data files from 1998 through 2005. However, none of these authors answered the fundamental question: Why does the low-frequency variability of temperature and salinity in the upper ocean in the southern California Current region, particularly off Baja California, increase southward? We hypothesized that the answer resides in basin-scale phenomena.

[3] This work attempts to explain the mixed layer (ML) temperature and ML salinity interannual variability off Baja California on the basis of IMECOCAL data files from 1997 through 2007. In particular, we studied the variability difference of these properties between the southern and the northern Baja California regions following *Lynn*'s [1967] and *Jeronimo and Gomez-Valdes*' [2006] findings. Our approach uses high-resolution (1 dbar) conductivity-temperature-depth (CTD) observations of the water column to calculate ML temperature and ML salinity. We also use satellite observations of sea surface height anomaly (SSH), and net heat flux (NHF) to illustrate the space and time relationships between mixed layer parameters and forcing mechanisms. In addition, time series of climate indices such as Pacific Decadal Oscillation (PDO) [*Mantua et al.*, 1997], Aleutian Low Pressure Index [*Beamish et al.*, 1997], Warm Water Volume (WWV) [*Meinen and McPhaden*, 2000], and North Pacific Gyre Oscillation (NPGO) [*Di Lorenzo et al.*, 2008] were employed in this study.

[1]Physical Oceanography Department, CICESE, Ensenada, Mexico.
[2]Now at Facultad de Ciencias, UNAM, Sisal, Mexico.

0148-0227/09/2008JC004793$09.00

[4] The rest of the text is divided into four sections. The second section provides background of the paper. The third section explains the data and the methods used. The fourth section presents the results. The discussion of the paper is presented in the fifth section. It will be demonstrated that at interannual timescales (1) the fundamental mode of variability of ML temperature is mainly explained by the difference in the variability of NHF between northern and southern Baja California, while (2) the fundamental mode of variability ML salinity is mainly explained by large-scale SSH.

2. Background

[5] Two water masses dominate the water mass spectrum at surface and subsurface levels in the coastal domain of the California Current System (CCS): subarctic water and equatorial water [*Sverdrup et al.*, 1942; *Tomczak and Godfrey*, 1994]. Low temperature, low salinity, and high nutrient concentration characterize the properties of the subarctic water [*Lynn and Simpson*, 1987]. On the other hand, high temperature, high salinity, and high nutrient concentration characterize the properties of the equatorial water [*Lynn and Simpson*, 1987]. Because the main physical processes in the CCS are time and space dependent [*Marchesiello et al.*, 2003; *Di Lorenzo et al.*, 2005], the mixing ratio of these water masses along the west coast of North America is a function of both time and space. Indeed, several studies of variability of the water column have showed that timescales from seasonal to decadal are very important in determining the distribution of properties of the CCS waters [*Huyer*, 2003].

[6] The mechanisms governing low-frequency variability of upper ocean temperature and salinity in the CCS have a remote as well as local origin [*Pares-Sierra and O'Brien*, 1989; *Miller*, 1996]. Numerical simulations of the dynamics and thermodynamics of the southern portion of the CCS revealed that the long-term changes in upper ocean temperature are controlled by NHF forcing at basin scale and advection of the mean currents at local scale [*Di Lorenzo et al.*, 2005]. However, no significant correlation was found between large-scale climate indices and upper ocean salinity changes. Large-scale changes in upper ocean temperature and SSH induced by Rossby waves associated to El Niño phenomenon have also been documented [*White et al.*, 1990; *Jacobs et al.*, 1994; *Lynn et al.*, 1995] in the northeastern Pacific. In this work, we use climate indices and the variability of SSH and NHF to search for remote and local influences.

[7] The PDO index has been associated with the first leading Empirical Orthogonal Functions (EOF) of observed North Pacific winter sea surface temperature (SST) [*Mantua et al.*, 1997]. It was in a cool phase from 1947 to 1976 and in a warm phase from 1977 to the mid-1990s [*Mantua and Hare*, 2002]. *Peterson and Schwing* [2003] suggest that there was a switch from the last warm phase to a cold phase in the PDO mode after the strong 1997–1998 El Niño. Using numerical models, it has been shown that decadal variations in the thermocline of the CCS are driven by a basin-scale change in Ekman pumping [*Miller*, 1996]. On the other hand, ENSO is the most important source of interannual variability in SSH and sea surface temperature (SST) in the northeast Pacific Ocean [*Chelton and Davis*, 1982; *Emery and Hamilton*, 1985; *Norton and McLain*, 1994; *Espinosa-Carreon et al.*, 2004]. Although the ENSO effect on the salinity variability remains unexplained [*Schneider et al.*, 2005], it has been shown that during strong El Niño salty and warm waters invade the upper ocean along the west coast of North America [*Durazo and Baumgartner*, 2002; *Lynn and Bograd*, 2002; *Chavez et al.*, 2002]. Besides the influence of ENSO in the interannual variability, effects on SSH, SST, and salinity field of events associated with Aleutian low atmospheric cyclogenesis have also been documented [*Emery and Hamilton*, 1985; *Huyer and Smith*, 1985].

[8] There are other possible sources of interannual variability linked to atmospheric forcing anomalies, among them, subarctic water enhancement events and delayed coastal upwelling events. With respect to the former phenomenon, during the summer of 2002 anomalous cold and fresh upper ocean water was observed along the west coast of North America [*Huyer*, 2003; *Durazo et al.*, 2005]. In particular, a cold and fresh halocline was found off Oregon and Vancouver Island [*Freeland et al.*, 2003] and negative temperature and salinity anomalies inside the California Current core were reported off southern California [*Bograd and Lynn*, 2003]. Also, *Durazo et al.* [2005] found low salinity and low temperature anomalies in the upper 100 m off Baja California, from July 2002 to April 2003, and *Perez-Brunius et al.* [2006] found anomalous low spiciness on σ_t 25.3 kg m^{-3} surface during their surveys of May 2002, June 2003, and May 2004, along the coastal waters of northern Baja California. With respect to the latter phenomenon, *Schwing et al.* [2006] showed a 2- to 3-month delay in the 2005 spring transition in the northern California Current. *Barth et al.* [2007] suggested that the delayed coastal upwelling at this region was associated with intraseasonal wind oscillations and the position of the jet stream. There are not reports of this phenomenon along the coast of Baja California.

3. Data and Methods

[9] IMECOCAL is an ongoing observational program that started during autumn 1997 and has carried out continuous quarterly surveys since. The surveys have been performed approximately in January, April, July, and October of each year, except April 1999 and October 2006. The sampling grid of IMECOCAL is a reduced CalCOFI grid, from lines 100–137, out to station 60, except lines 117 and 120 in which three more offshore stations were occupied (Figure 1). For a description of the CalCOFI sampling grid see *Lynn and Simpson* [1987]. *Durazo and Baumgartner* [2002] describe the IMECOCAL data collected between 1997 and 1999 and *Soto-Mardones et al.* [2004] give a description of the data collected between 2000 and 2002.

[10] In the IMECOCAL grid, spacing between stations is approximately 37 km and spacing between hydrographic lines is approximately 74 km. At each station, CTD/rosette casts are taken from the surface to a minimum depth of 1000 m, using a Seabird CTD. Temperature and conductivity sensors are factory calibrated prior to each survey. A total of 36 quarterly IMECOCAL's surveys were used in the present study, from October 1997 to January 2007. The vertical resolution of each CTD profile was 1 dbar.

[11] To obtain ML temperature and ML salinity, we first calculated the quasi isothermal layer depth ($h_\theta(\vec{x}, t)$) and the quasi isohaline layer depth ($h_S(\vec{x}, t)$). These layers depths,

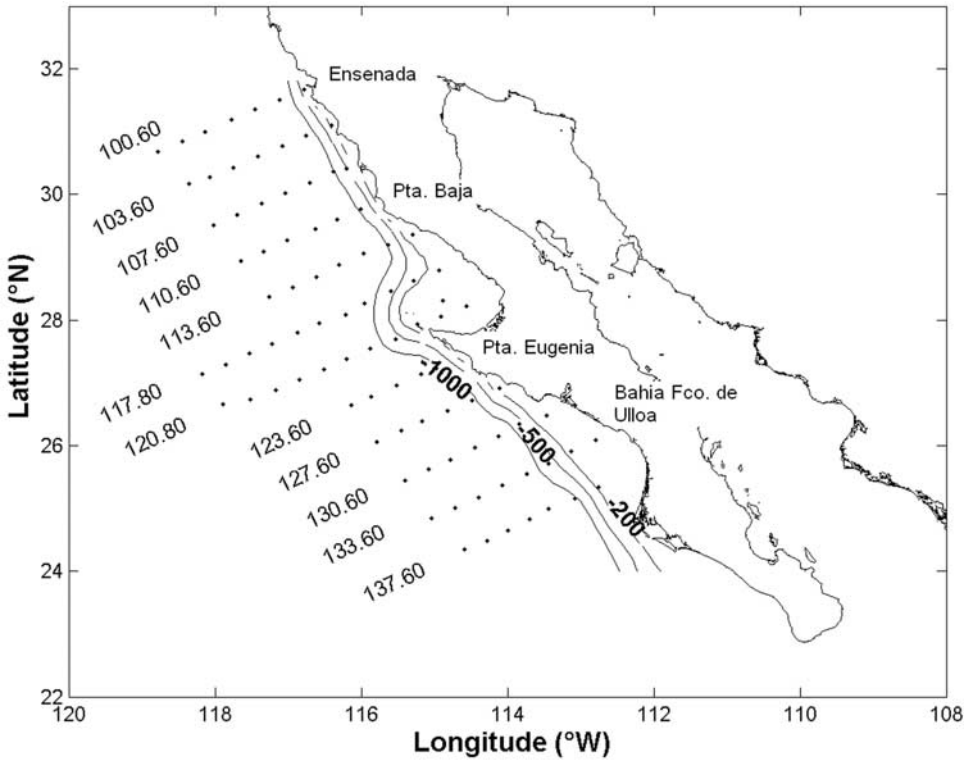

Figure 1. Study area. Black points represent the 93-station pattern occupied by the IMECOCAL program since 1997. Depth contours are in m.

$h_\theta(\vec{x}, t)$ and $h_S(\vec{x}, t)$, were computed for each station and for each survey following *Kara et al.*'s [2000] methodology, using a $\Delta\theta$ criterion for potential temperature and a ΔS criterion for salinity. $h_\theta(\vec{x}, t)$ and $h_S(\vec{x}, t)$ showed both time and space variations. After the depths were computed, we integrated the thermodynamic variables from the bottom of the layer to the sea surface for each profile,

$$ML\ temperature(\vec{x}, t) = \frac{1}{h_\theta} \int_{-h_\theta}^{0} \theta(\vec{x}, t) dz, \quad (1)$$

$$ML\ salinity(\vec{x}, t) = \frac{1}{h_s} \int_{-h_s}^{0} S(\vec{x}, t) dz, \quad (2)$$

where $\theta(\vec{x}, t)$ and $S(\vec{x}, t)$ are potential temperature and salinity, respectively.

[12] Because the IMECOCAL sampling of temperature and salinity is inhomogeneous, we used optimal interpolation to obtain gridded data. Optimal interpolation was implemented following the Gauss-Markov theorem [*Davis*, 1985; *Le Traon*, 1990]. The alongshore/cross-shore decorrelation length scale used in the mapping is 110 km/74 km as determined by *Jeronimo and Gomez-Valdes* [2006]. To obtain the variability fields, EOFs analysis was applied to time series anomalies of the gridded data of ML temperature and ML salinity.

[13] The set of EOFs for the quarterly anomalies of ML temperature and ML salinity was obtained as follows:

$$X' = X - \langle X \rangle, \quad (3)$$

where $\langle X \rangle$ is the mean of the time series at station_i of each mixed layer parameter, X is the mixed layer parameter at station_i and time t, and X' is the anomaly of each mixed layer parameter at station_i and time t. In addition, the set of EOFs for the nonseasonal (interannual) anomalies of the ML temperature and ML salinity was obtained following *Espinosa-Carreon et al.* [2004] and *Doney et al.* [2007] in the form:

$$X'' = X' - \{A_1(\vec{x}) \cos(\varphi_1 t - f_1) + A_2(\vec{x}) \cos(\varphi_2 t - f_2)\}, \quad (4)$$

where A_1 and A_2 are the annual and semiannual amplitudes for each time series, respectively, φ_1 and φ_2 are the frequencies of annual and semiannual harmonic, respectively, f_1 and f_2 are the phases of annual and semiannual harmonic, respectively, and t is the time. The fitting of each station record was done by regression analysis using the principle of least squares.

[14] To explain the variability of ML temperature and salinity, we also used satellite data records of SSH and NHF. Time series of SSH, from TOPEX and ERS 1–2 satellites, spanning from January 1994 to August 2002, were obtained from Southampton Oceanography Center. Additionally, time series of SSH, from Jason-1, spanning from September 2002 to January 2007, were obtained from

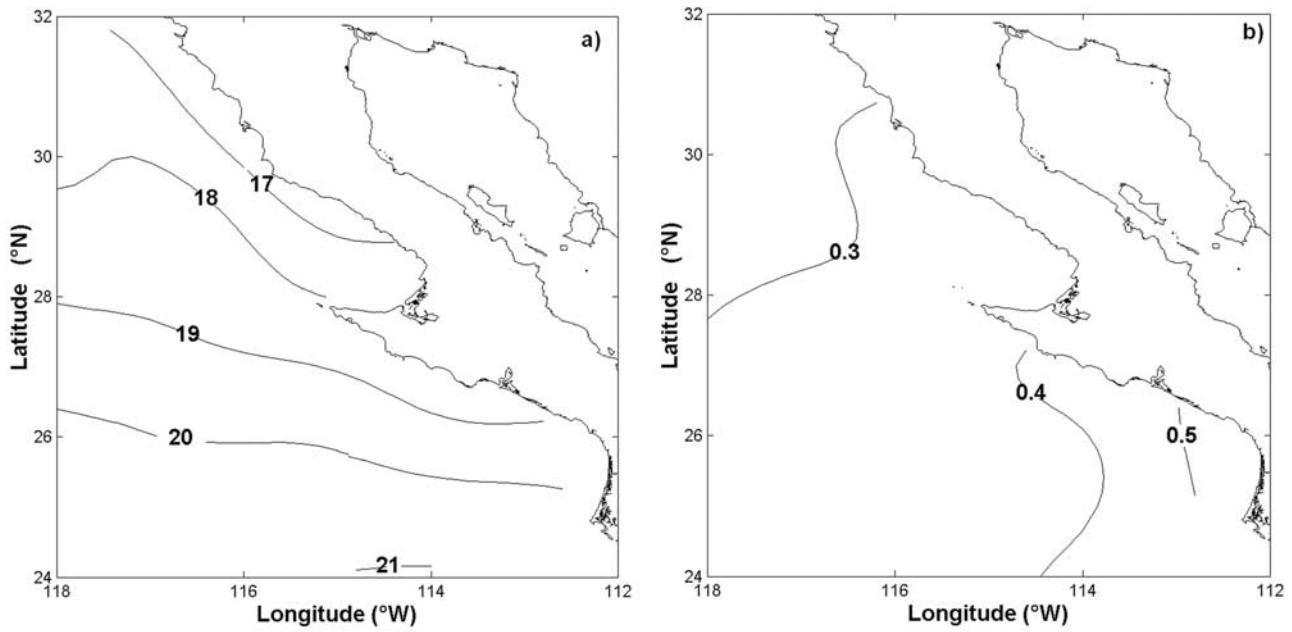

Figure 2. Mean and standard error of mixed layer temperature (°C) from IMECOCAL data from July 1998 to January 2007.

Radar Altimeter Database System (RADS). The sampling period is 10 days for TOPEX and Jason-1, and 35 days for ERS 1–2. The separation among tracks is 160 km for TOPEX and Jason-1, and 70 km for ERS 1–2. Time series from January 1997 to January 2007 of NHF were obtained from the NCEP/NCAR Reanalysis project. We used *Jeronimo and Gomez-Valdes*' [2006] optimal interpolation methodology to obtain gridded data of SSH and NHF. EOFs analysis was also performed for SSH and NHF values, using the same methodology as for the ML temperature and ML salinity interannual anomalies described above.

[15] To quantify the relationships among hydrographic parameters and forcing mechanisms, we computed the correlation coefficients between the principal component (PC) time series of ML parameters and the PC time series of satellite products. The same procedure was performed to calculate correlation coefficients between hydrographic parameters and climate indices. Significance analysis was performed by the method described by *Emery and Thomson* [2001]. We also computed the projection of each EOF obtained from satellite product on each EOF obtained from ML parameter by the method described by *Wang and Walsh* [1976]. This method consists of computing the inner product between the *i*th mode from satellite product and the *j*th mode from mixed layer parameter, and standardizing by multiplication of the norm of each vector. A projection coefficient of 1 means the vectors are parallel; that is, with the same structure.

4. Results

4.1. Mean Fields

[16] A total of 36 surveys were used in the analysis, however since the strong 1997–1998 El Niño [*McPhaden*, 1999] could create bias in the mean fields, we did not include the data from the October 1997 survey nor from the January 1998 survey to obtain basic statistics of hydrographic data. For this reason the mean and standard deviation of ML temperature and ML salinity for each station was calculated from the remaining set of 34 surveys. We also calculated the standard deviation of the mean (standard error) which describes the precision of the mean [*Taylor*, 1997]. The standard error is given by $\sigma_m = \sigma/\sqrt{N}$, where σ is the standard deviation and N is the number of data. Once we had the basic statistics for each station, we proceeded to perform optimum interpolation and to calculate σ_m.

[17] The mean and the standard error for the ML temperature are shown in Figure 2. The 17°C isotherm runs parallel to the coast because of coastal upwelling. The sharp southward bend of the 18°C isotherm also suggests coastal upwelling. South of Punta Eugenia, the bending of the isotherms is less pronounced. The maximum temperature (20°C) occurs in the transition domain off southern Baja California while the minimum (17°C) occurs in the coastal domain off northern Baja California. We are using the domain classification of *Lynn and Simpson* [1987] to describe the observations. The variability (standard error) increases monotonically southward.

[18] The mean and the standard error for the ML salinity are shown in Figure 3. The overall mean salinity (33.6) occurs off Punta Eugenia. In the 33.5 to 33.7 salinity belt, the isohalines have zonal distribution, except for the eastern portion of the 33.5 isohaline that runs parallel to the coast as an indication of southward flow. South of Punta Eugenia, the mean isohalines run along a meridian direction. The salinity decreases from 33.9 to 33.5, monotonically northward, with a greater variability in the southern part than in the northern one. It is noteworthy that there is a relatively high-variability center off northern Baja California.

4.2. Quarterly Anomalies

[19] For this case, the EOFs analysis of ML temperature and ML salinity was performed using the full, unfiltered

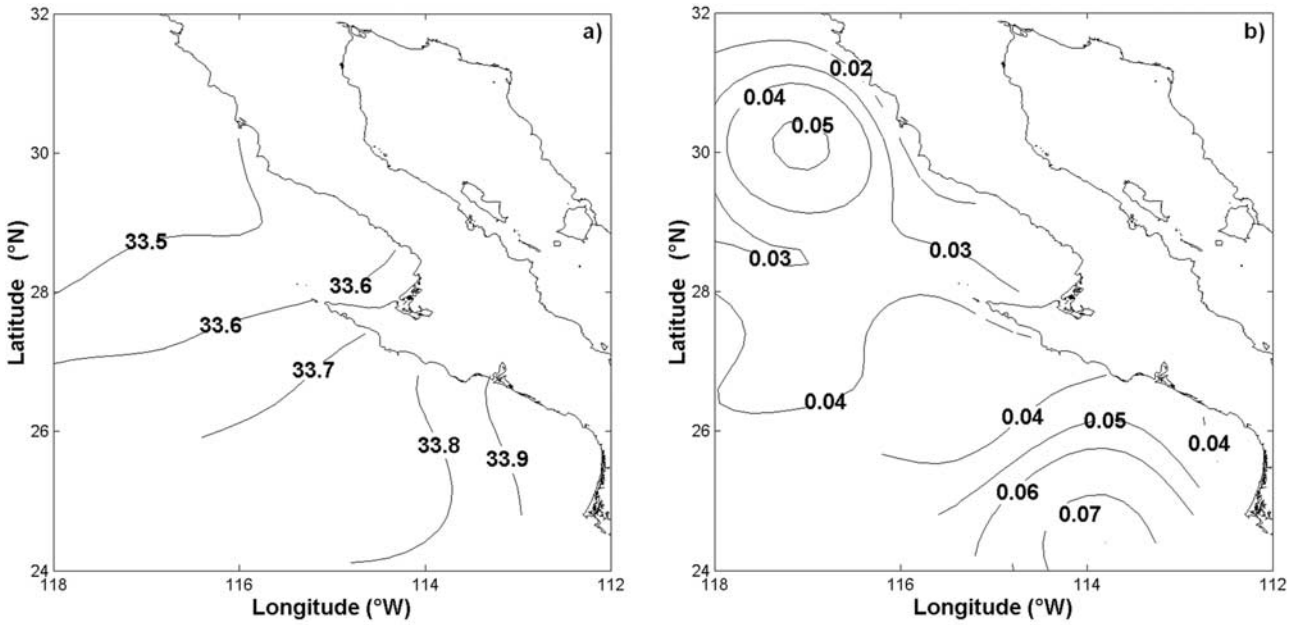

Figure 3. (a, b) Mean and standard error of mixed layer salinity from IMECOCAL data from July 1998 to January 2007.

anomalies (equation (3)), therefore the resulting orthogonal functions contains seasonal and nonseasonal variability. According to our main objectives, only the first leading mode (EOF-1) of each variable is presented in this section.

[20] Figure 4 shows the spatial and temporal patterns of the first leading EOFs of ML temperature and ML salinity anomalies. The EOF-1 of ML temperature accounts for 86% of the total variance. Its spatial pattern shows a single-signed loading, in which the variability increases southward. The corresponding PC shows an annual cycle with the positive value occurring in October and the negative value occurring in April. There is also an event of high positive amplitude associated with the 1997–1998 El Niño. The EOF-1 of ML salinity accounts for 65% of the total variance. Its spatial pattern shows a single-signed loading, in which the variability increases southward. Its corresponding PC time series shows high positive values associated with the 1997–1998 El Niño. It shows also predominantly positive values from 1998 until 2003 and predominantly negative values from 2003 until 2006.

4.3. Interannual ML Temperature and ML Salinity

[21] In this section, the interannual variations of the ML temperature and ML salinity fields are addressed. The EOFs analysis was performed on the interannual anomalies (equation (4)). Because most of the variability of temperature and salinity was captured by the first three leading modes with 82% of the total variance for both ML temperature and ML salinity, we restrict our discussion to the patterns of these three modes.

[22] The spatial and temporal patterns of the first three leading EOFs of the ML temperature anomalies are shown in Figure 5. The EOF-1 accounts for 71% of the explained variance. The spatial pattern shows a single-signed loading, in which the variability increases southward. Its corresponding PC time series shows interannual variability with an abrupt cooling from January 1998 to January 1999 when the temperature falls 4.5°C off southern Baja California and 3.2°C off northern Baja California. The lowest ML temperature anomaly is registered in January 2006. This low-temperature event was reported by *Peterson et al.* [2006]. The EOF-2 accounts for 6% of the total variance. The spatial pattern shows a double-signed loading, separating the northern region from the southern region off Punta Eugenia. Its corresponding PC time series shows that the interannual variability was higher for the period 1998–2002 than for the period 2002–2005. This result indicates a nonstationary process. The EOF-3 accounts for 5% of the explained variance. The spatial pattern shows a double-signed loading, separating the coastal domain from the transition one. This mode might be associated with coastal upwelling. Its corresponding PC time series shows an annual cycle between 1998 and 2002, followed by an upward trend afterward.

[23] The dominant EOFs of the ML salinity anomalies are shown in Figure 6. The EOF-1 accounts for 61% of the total variance. The spatial pattern shows a single-signed loading, in which the variability increases southward. It is noteworthy a tongue of high variability intruding northward off northern Baja California. The PC time series shows two distinctive regimes, with the transition centered in 2002. An abrupt freshening event occurs between January 1998 and January 1999 when the salinity falls 0.8 off southern Baja California and 0.5 off northern Baja California. Although of lesser magnitude, another abrupt freshening event also occurs between January 2002 and January 2003. The latter freshening event is perceptible until 2006. The EOF-2 accounts for 12% of the explained variance. The spatial pattern shows a double-signed distribution, separating the northern region from the southern region off Punta Eugenia, and a center of high variability off northern Baja California. The PC time series shows a peak in January of 2003. The EOF-3 accounts for 9% of the total variance. Its spatial pattern shows two

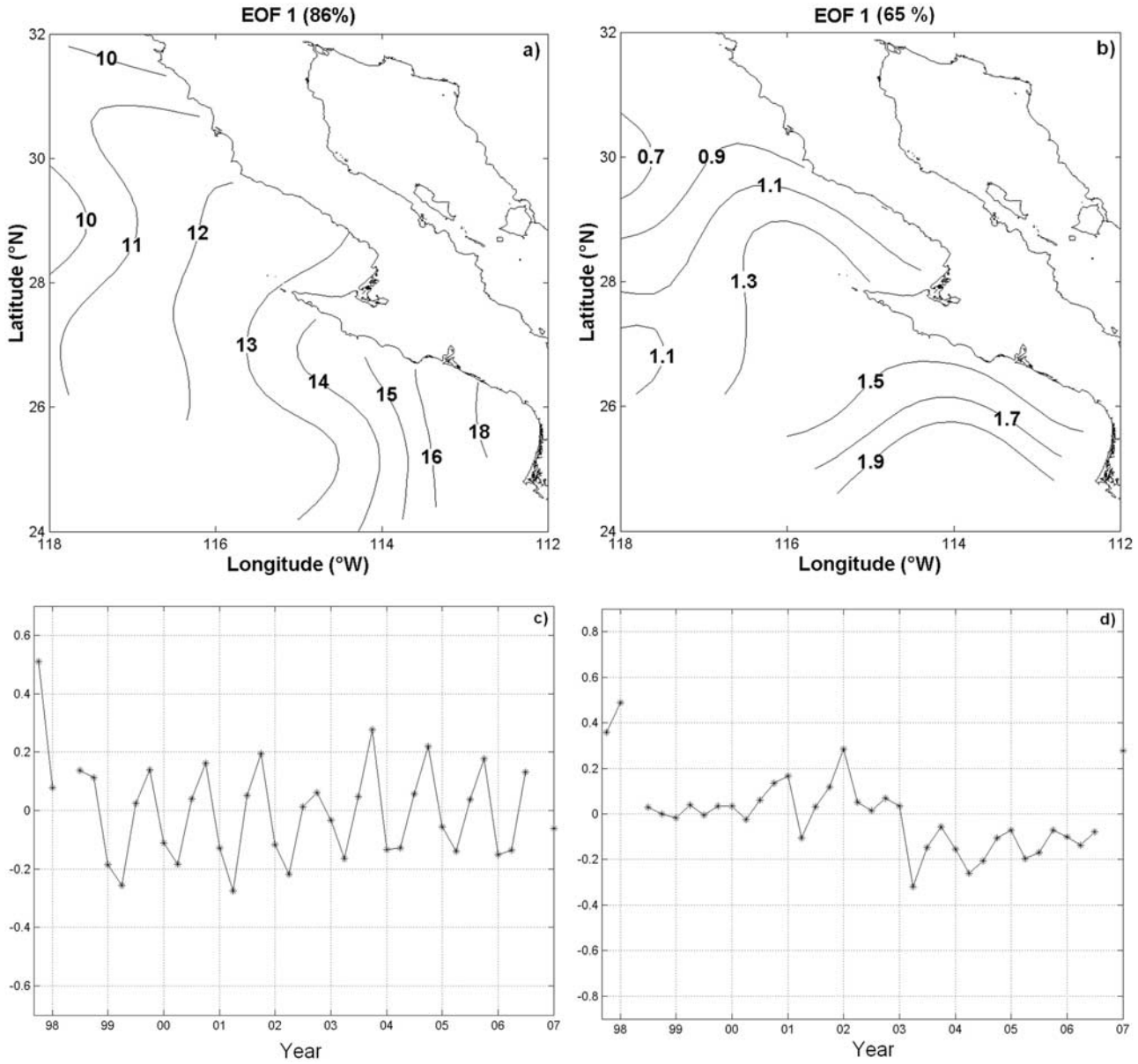

Figure 4. (a, b) The spatial patterns of the first leading EOFs of mixed layer temperature and salinity quarterly anomalies from IMECOCAL data from October 1997 to January 2007. (c, d) The principal components of each mode. Unit of temperature is °C.

high-variability centers, one off southern Baja California that is not conspicuous in the EOF-2, and the other off northern Baja California. Its PC time series is similar to the PC time series of EOF-2.

[24] EOFs analysis was also performed on the interannual anomalies without 1997–1998 El Niño (not shown here). The distributions of the total variance in the two experiments (one with El Niño and the other without it) were different from each other, as expected, and so were the spatial pattern. The first leading modes of both variables were more/less energetic with El Niño present/absent. Nevertheless, the single-signed loading pattern was invariable in both experiments. In the case of ML salinity, the peculiar features of the spatial patterns off Punta Eugenia observed in Figure 6 were induced by the 1997–1998 El Niño. The second leading modes of both variables were more/less energetic with El Niño absent/present, but the double-signed loading patterns were still the same; similar results were observed in the third leading mode.

[25] Hence the results of the sensitivity analysis without the 1997–1998 El Niño confirm our statement that the first mode of variability as extracted by EOFs analysis is the fundamental mode of interannual variability of ML temperature and ML salinity.

4.4. Interannual SSH and NHF

[26] In this section the interannual SSH and NHF changes are presented. The EOFs analysis was performed on the interannual anomalies (equation (4)) over the period January 1997 to January 2007 for SSH and over the period October

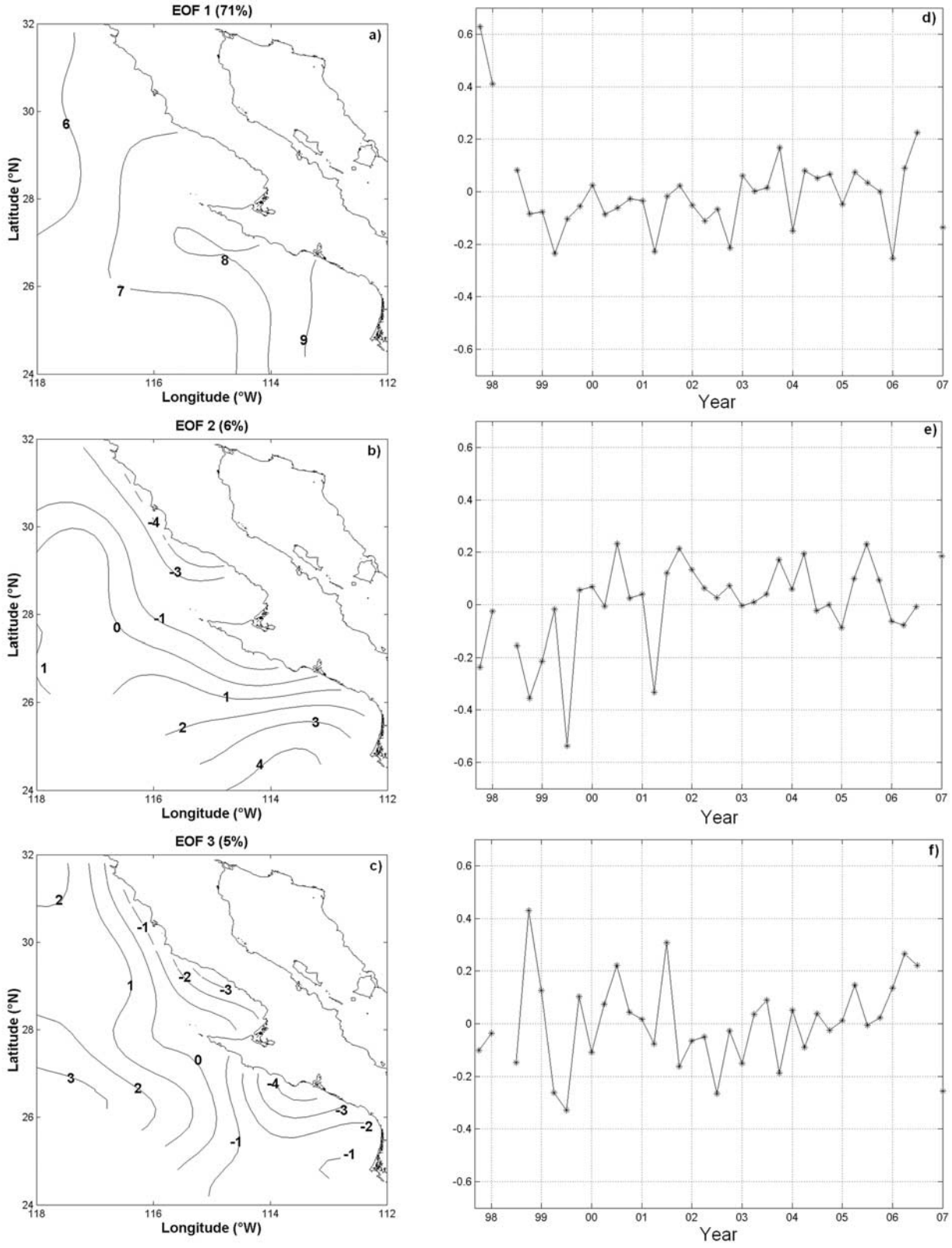

Figure 5. (a, b, c) The spatial patterns of the first three leading EOFs of mixed layer temperature interannual anomalies from IMECOCAL data from October 1997 to January 2007. (d, e, f) The principal components of each mode. Unit of temperature is °C.

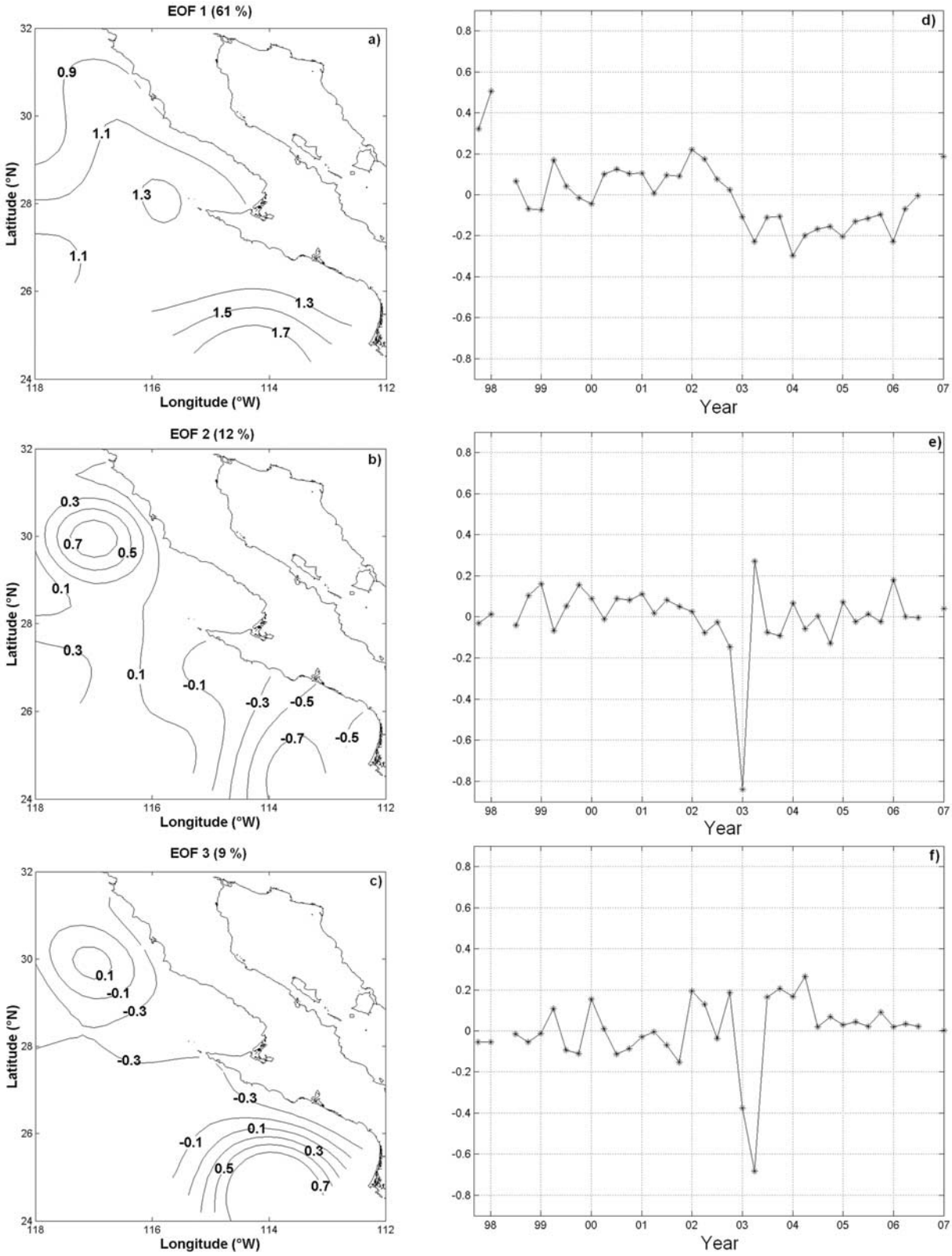

Figure 6. The same as Figure 5, but for mixed layer salinity interannual anomalies.

1997 to January 2007 for NHF. Figure 7 shows the dominant EOFs of the SSH anomalies, that accumulate 71% of the explained variance. The EOF-1 accounts for 59% of the total variance. Its spatial pattern shows a single-signed distribution with the highest variability located in the coastal domain of southern Baja California. It is noteworthy the great richness of mesoscale features in this structure. Its temporal pattern shows an abrupt rise and fall oscillation of sea level from

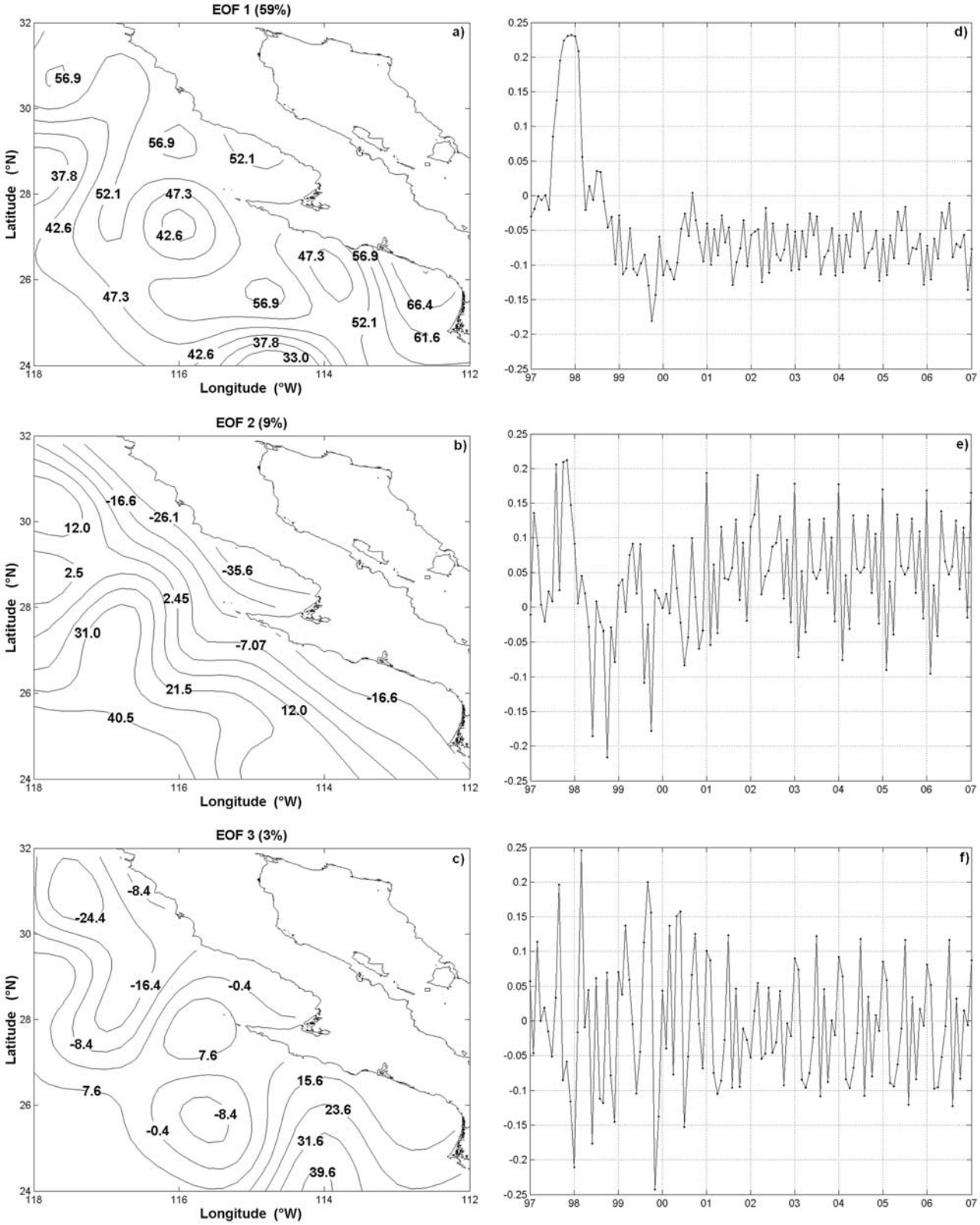

Figure 7. (a, b, c) The spatial patterns of the first three leading EOFs of SSH interannual anomalies from January 1997 to January 2007. (d, e, f) The principal components of each mode. Unit of SSH is cm.

December 1997, positive maximum (0.24) amplitude, to October 1999, negative maximum amplitude (−0.18), because of the El Niño–La Niña cycle. The EOF-2 accounts for 9% of the total variance. Its spatial pattern shows a double-signed distribution, separating the coastal domain from the transition one. This pattern is similar to the one reported by *Lynn and Simpson* [1987] for the standard deviation of dynamic height. Its corresponding PC time series shows that

El Niño–La Niña cycle perturbs the mode from 1997 to 1999, and then the time series oscillates until the winter 2007. From the winter 2000 to the winter 2003 there is conspicuous positive trend. The EOF-3 accounts for 3% of the explained variance. Its spatial pattern shows a double-signed distribution separating the north region from the south region off Punta Eugenia. This mode appears to be related to steric anomalies. Its corresponding temporal pattern shows an oscillatory character.

[27] EOFs analysis of SSH was also performed on the interannual anomalies without the 1997–1998 El Niño (not shown here), using a time series of SSH for the period between January 1994 and January 2007. For EOF-1, the percentage of the total variance for the experiment with El Niño present/absent was higher/lower than for the experiment without it. The spatial patterns were dissimilar. Without El Niño experiment, the upper ocean mesoscale features documented by several authors were more conspicuous than with El Niño. The complete time series reveled that the 1997–1998 El Niño peaked in December 1997 off Baja California. *Bograd and Lynn* [2001] reported that this event peaked in February 2008 off Southern California. The patterns of EOF-2 and EOF-3 for both experiments were practically the same.

[28] Figure 8 shows the dominant EOFs of the NHF interannual anomalies. These EOFs accumulate 75% of the explained variance. The EOF-1 accounts for 40% of the total variance. Its spatial pattern shows a single-signed loading, in which the variability increases southward. This mode shows that the NHF variability is higher off southern than off northern Baja California. Its corresponding PC time series shows a predominance of an annual cycle, but an abrupt NHF down shift occurs between January 1998 and January 1999 associated with El Niño–La Niña cycle. During this period, NHF falls 90 W m^{-2} off southern Baja California and 70 W m^{-2} off northern Baja California. The EOF-2 accounts for 20% of the explained variance. The spatial pattern shows a double-signed loading, separating the variability off northern Baja California from the variability off southern Baja California. This mode appears to be dominated by the advection of cold water due to the main core of the California Current as described by *Lynn and Simpson* [1987]. The temporal pattern is oscillatory with the exception of the period 2002–2004 in which positive values prevail. The EOF-3 accounts for 15% of the total variance. Its spatial pattern shows a double-signed distribution separating the coastal domain from the transition one. Like the EOF-3 of ML temperature, this mode might be associated with coastal upwelling. Its corresponding PC time series shows predominantly positive values between 2000 and 2004, the rest of the record is oscillatory.

4.5. Correlations Between Mixed Layer Properties, SSH, NHF, and Climate Indices

[29] SSH and NHF were used as variable proxies to explain the variability of the mixed layer properties. To evaluate the possible interrelationship between ML temperature and SSH/NHF, we calculated the correlation coefficients between the PC times series of ML temperature and the PC time series of SSH/NHF. The same correlation analysis was performed for ML salinity and SSH/NHF. Projection coefficient analysis between the EOF of the ML properties and the EOFs of satellite products was also performed.

[30] Table 1 shows the correlation analysis results, correlations values greater than 0.35 are significant at the 95%. The PC corresponding to the EOF-1 (PC-1) of the ML temperature anomalies is significantly correlated (0.5) with the PC-1 of NHF. The PC-1 of the ML salinity anomalies is significantly correlated (0.5) with the PC-2 of SSH. The projection coefficient, on the other hand, between the EOF-1 of the ML temperature and the EOF-1 of SSH is high (0.7), but it is higher (0.8) with the EOF-1 of NHF. Corresponding projection values for the EOF-1 of ML salinity are identical.

[31] Concerning the second mode of the ML temperature anomalies, there is a correlation between the PC-2 of ML temperature and the PC-3 of SSH. There is high projection coefficient among the EOF-2 of ML temperature and both the EOF-3 of SSH and the EOF-2 of NHF. Regarding the second mode of the ML salinity anomalies, there is not a significant correlation with either SSH or NHF. The PC-3 of ML temperature is correlated with the PC-3 of SSH. There is also high projection coefficient among the EOF-3 of ML temperature and both the EOF-2 of SSH and the EOF-3 of NHF, while the PC-3 of ML salinity is significantly correlated with the PC-3 of NHF. There is also high projection coefficient between the EOF-3 of ML salinity and the EOF-2 of NHF.

[32] Table 2 shows the correlation coefficients among the PCs of the mixed layer parameters and climate indices, correlations values greater than 0.35 are significant at the 95% level for all climate indices except ALPI, for which significance threshold is 0.63 at the 95% level. The PC-1 of ML temperature is only significantly correlated with WWV, while the PC-1 of ML salinity is significantly correlated not only with WWV but also with PDO and ALPI. PC-2 of ML temperature is significantly correlated with WWV. It is noteworthy that mode 3 of ML temperature is not correlated with any of the climate indices; the same applies to mode 3 of ML salinity although it is correlated with ALPI in the limit of significance. Table 2 also shows the correlation coefficients between SSH/NHF and climate indices. PDO and ALPI show more influence on the SSH and NHF modes than WWV.

5. Discussion and Conclusions

[33] From data collected on 36 IMECOCAL surveys over a 10-year period (1997–2007), the interannual variability of the ML temperature and ML salinity off Baja California was presented. The mean and standard error of the ML temperature and ML salinity fields are consistent with those of *Lynn* [1967] for the CalCOFI data 13-year mean (1950–1967) at 10 m depth. The maximum ML temperature off northern Baja California (18.0°C) has the same magnitude as the one reported by *Bograd et al.* [2001]. The standard error distribution of both ML temperature and ML salinity shows that the variability of the upper ocean temperature and salinity increases southward. Those patterns were reproduced by the EOFs analysis of both parameters. The seasonality of the ML temperature is more intense than the seasonality of ML salinity. The study of the seasonal variability of both variables will be published in the Journal of Geophysical Research. We focus here on the interannual variability timescale.

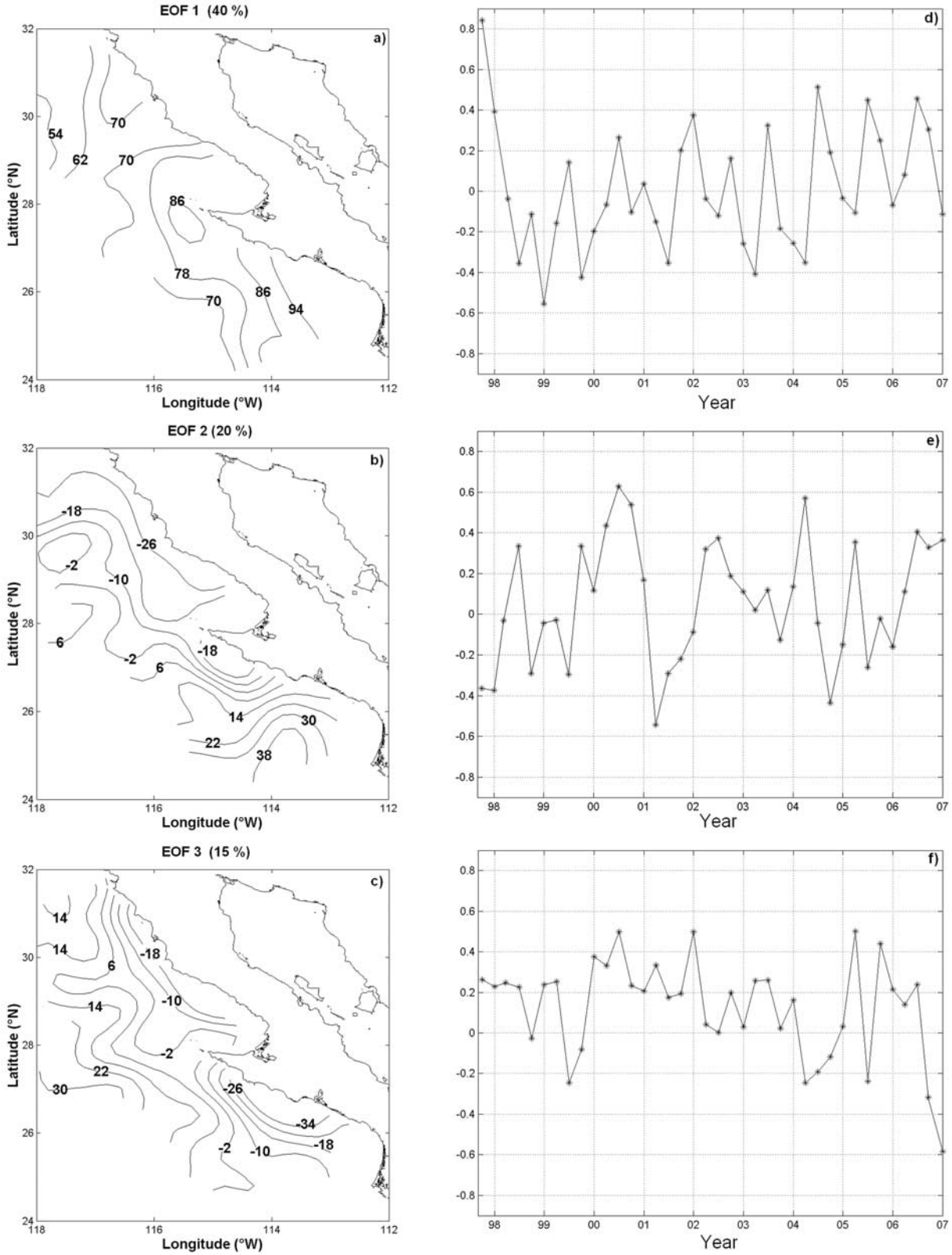

Figure 8. The same as Figure 7, but for NHF interannual anomalies from October 1997 to January 2007. Unit of NHF is W m^{-2}.

Table 1. Correlation Coefficients Between Mixed Layer Temperature and Sea Surface Height Anomaly and Net Heat Flux as Well as Correlation Coefficients Between Mixed Layer Salinity and Sea Surface Height Anomaly/Net Heat Flux[a]

	Mixed Layer Temperature			Mixed Layer Salinity		
	1	2	3	1	2	3
			Sea Surface Height Anomaly			
1	−0.2(0.7)	0.2(0.2)	−0.2(0.1)	0.4(0.8)	−0.1(0.1)	−0.2(0.2)
2	0.2(0.1)	−0.3(0.3)	0.2(0.7)	0.5(0.1)	−0.1(0.2)	0.0(0.0)
3	−0.4(0.1)	0.4(0.8)	−0.4(0.4)	−0.3(0.2)	0.1(0.4)	−0.2(0.5)
			Net Heat Flux			
1	0.5(0.8)	−0.2(0.0)	0.0(0.1)	0.4(0.8)	0.3(0.0)	0.0(0.1)
2	−0.1(0.1)	−0.3(0.8)	−0.1(0.2)	0.2(0.1)	0.3(0.4)	−0.2(0.7)
3	0.1(0.0)	−0.1(0.2)	0.2(0.8)	−0.1(0.1)	−0.3(0.4)	−0.4(0.1)

[a]Projection coefficients are included in the parentheses.

[34] The spatial pattern of the first leading EOF of ML temperature shows a single-signed loading with variability increasing southward. The same pattern was shown in the works of *Lynn* [1967] and *Jeronimo and Gomez-Valdes* [2006], who used different sets of data and methodologies. The projection coefficient of EOF-1 of ML temperature with the EOF-1 of SSH is high (0.7), as it is also high with the EOF-1 of NHF. However, the PC-1 of ML temperature is only highly correlated with the PC-1 of NHF. Therefore our conclusion is that the leading mode of ML temperature variability off Baja California is mainly explained by the NHF variability. The importance of ENSO in determining its interannual variability is highlighted by the significant correlation between the PC-1 of ML temperature and WWV. The 1997–1999 El Niño–La Niña cycle generated an abrupt cooling event.

[35] The spatial pattern of the first leading EOF of ML salinity shows a single-signed loading with variability increasing southward. The EOF-1 of ML salinity is parallel not only to the EOF-1 of SSH but also to the EOF-1 of NHF. However, the PC-1 of ML salinity is highly correlated with the PC-2 of SSH. Because NHF is linked to SSH, it is more likely that the leading mode of ML salinity is connected to SSH. Therefore our conclusion is that the leading mode of ML salinity is mainly explained by SSH variability. The 1997–1999 El Niño–La Niña cycle generated also an abrupt freshening event. The highest salinity is reached in January of 1998. *Durazo and Baumgartner* [2002] documented the hydrology off Baja California of that cycle. They found that anomalous warmer and saltier waters were transported from the south via the California Undercurrent. It is also important to note the change from January 2002 to January 2003; this freshening event spans a period of 4 years (2002–2006). This event might be associated with an anomalous invasion of subarctic water that started during the summer of 2002, as it has documented by several investigators [*Freeland et al.*, 2003; *Bograd and Lynn*, 2003; *Durazo et al.*, 2005; *Perez-Brunius et al.*, 2006]. That likely explanation suggests that the anomalous event is related to a large-scale process. Moreover, the significant correlation between the PC-1 of ML salinity and PDO, ALPI, and WWV suggests that this mode is strongly influenced by basin-scale processes.

[36] The EOF-2 of ML temperature and the EOF-2 of ML salinity show in its spatial pattern a double-signed structure, separating the northern region from the southern region. The EOF-2 of ML temperature is parallel to the EOF-3 of SSH and the EOF-2 of NHF. On the other hand, the PC-2 of ML temperature is better correlated with the PC-3 of SSH than with any PC of NHF. Thus the third mode of SSH explains the second mode of ML temperature. Concerning EOF-2 of ML salinity, its corresponding PC is better correlated with NHF than with SSH. *Durazo and Baumgartner* [2002] and *Jeronimo and Gomez-Valdes* [2006] suggested that the confluence of the two major water masses occurs off Punta Eugenia. So it appears that these patterns are related to local variations of SSH and NHF.

[37] The EOF-3 of ML temperature shows in its spatial pattern a double-signed structure, separating the coastal domain from the transition one as *Lynn and Simpson* [1987] found for the dynamic height anomaly. Hence, the most likely mechanisms that explain the mode are local circulation, mesoscale eddies and coastal upwelling. The EOF-3 is parallel to the EOF-2 of SSH and to the EOF-3 of NHF. The spatial pattern shows two regions attributable to intense upwelling, one at northern Baja California (Punta Baja) and the other at southern Baja California. The former has been documented by *Barton and Argote* [1980] and *Zaytsev et al.* [2003] and the latter by *Zaytsev et al.* [2003]. The PC-3 of ML temperature is correlated with the PC-2 of SSH and with the PC-3 of NHF. EOF-3 and EOF-2 of ML salinity have common features. Both show centers of high variability, which might be associated with mesoscale surface eddies reported in the literature [*Strub and James*, 2000; *Soto-Mardones et al.*, 2004; *Espinosa-Carreon et al.*, 2004; *Jeronimo and Gomez-Valdes*, 2007].

Table 2. Correlation Coefficients

	Mixed Layer Temperature			Mixed Layer Salinity			Sea Surface Height Anomaly			Net Heat Flux		
	1	2	3	1	2	3	1	2	3	1	2	3
Pacific Decadal Oscillation	−0.3	0.2	0.0	−0.4	−0.1	0.0	0.4	−0.5	0.1	0.4	0.0	0.3
Aleutian Low Pressure Index	0.1	0.5	−0.5	0.8	−0.4	−0.6	0.5	0.5	−0.9	−0.4	−0.2	0.1
Warm Water Volume	0.5	−0.5	0.1	0.5	−0.2	0.0	−0.2	0.4	−0.6	−0.3	0.2	0.1

[38] Coastal Upwelling Indices (CUI) from NOAA Fisheries Science Center Environmental Research Division at three locations 30°N, 27°N, and 24°N for the period 1997–2007 were correlated with the PCs of ML temperature, ML salinity, and NHF, at interannual timescales. The highest correlation (0.8) was between the CUI at 27°N and the PC-3 of NHF; for this CUI a significant correlation (0.5) with the PC-3 of ML temperature was also found. These results confirm the hypothesis that the EOF-3 of ML temperature is related to coastal upwelling.

[39] NPGO is a climate index elaborate by *Di Lorenzo et al.* [2008]. We calculated the correlation coefficient between NPGO and each one of the PC time series obtained in this work. For the correlation analysis between NPGO and SSH, the time series of both spanned from January 1994 to January 2007. The highest correlation (0.9) was between NPGO and SSH-2. Hence, our EOFs analysis of SSH at local scale is consistent with the EOFs analysis of SSH at basin scale by *Di Lorenzo et al.* [2008]. The other results from the correlation analysis are also consistent with our conclusions.

[40] The first leading mode of ML temperature variability is mainly controlled by local forcing, while the first leading mode of ML salinity variability is mainly controlled by basin-scale variations in upper ocean dynamics. But ENSO is important for both, which implies that the Equatorial Pacific signal modulated the upper water mass interannual variability. The lower ML temperature mode is a suitable proxy for coastal upwelling process. Giving the fact that coastal upwelling is the most important mechanisms to enhance primary productivity off Baja California [*Wang and Walsh*, 1976]; our results are very promising for the study of the distribution of biological properties.

[41] **Acknowledgments.** This work was supported in part by grants from CONACyT (Mexico): 42569, 23947, and 47044, and from SEMARNAT-CONACyT: 23804. We thank captain and crew of the R/V *Francisco de Ulloa* of CICESE. Jorge Reyes de la Gala edited the paper. We also thank two anonymous reviewers for their very helpful suggestions that improved the paper.

References

Auad, G., A. Pares-Sierra, and G. K. Vallis (1991), Circulation and energetics of a model of the California Current, *J. Phys. Oceanogr.*, *21*, 1534–1552, doi:10.1175/1520-0485(1991)021<1534:CAEOAM>2.0.CO;2.

Barth, J. A., B. A. Menge, J. Lubchenco, F. Chan, J. M. Bane, A. R. Kirincich, M. A. McManus, K. J. Nielsen, S. D. Pierce, and L. Washburn (2007), Delayed upwelling alters nearshore coastal ocean ecosystems in the northern California current, *Proc. Natl. Acad. Sci. U. S. A.*, *104*, 3719–3724.

Barton, E. D., and M. L. Argote (1980), Hydrographic variability in an upwelling area off Northern Baja California in June, 1976, *J. Mar. Res.*, *38*, 631–649.

Beamish, R. J., C. E. Neville, and A. J. Cass (1997), Production of Fraser River sockeye salmon (*Oncorhynchus nerka*) in relation to decadal-scale changes in the climate and the ocean, *Can. J. Fish. Aquat. Sci.*, *54*, 543–554, doi:10.1139/cjfas-54-3-543.

Bograd, S. J., and R. J. Lynn (2001), Physical-biological coupling in the California Current during the 1997–1999 El Niño–La Niña cycle, *Geophys. Res. Lett.*, *28*, 275–278, doi:10.1029/2000GL012047.

Bograd, S. J., and R. J. Lynn (2003), Anomalous subarctic influence in the southern California Current during 2002, *Geophys. Res. Lett.*, *30*(15), 8020, doi:10.1029/2003GL017446.

Bograd, S. J., T. K. Chereskin, and D. Roemmich (2001), Transport of mass, heat, salt, and nutrients in the southern California Current System: Annual cycle and interannual variability, *J. Geophys. Res.*, *106*, 9255–9275, doi:10.1029/1999JC000165.

Chavez, F. P., C. A. Collins, A. Huyer, and D. L. Mackas (2002), El Niño along the west coast of North America, *Prog. Oceanogr.*, *54*, 1–5, doi:10.1016/S0079-6611(02)00040-X.

Chelton, D. B., and R. E. Davis (1982), Monthly mean sea-level variability along the west coast of North America, *J. Phys. Oceanogr.*, *12*, 757–784, doi:10.1175/1520-0485(1982)012<0757:MMSLVA>2.0.CO;2.

Davis, R. E. (1985), Objective mapping by least squares fitting, *J. Geophys. Res.*, *90*, 4756–4777, doi:10.1029/JC090iC03p04756.

Di Lorenzo, E., A. J. Miller, N. Schneider, and J. C. McWilliams (2005), The warming of the California Current System: Dynamics and ecosystem implications, *J. Phys. Oceanogr.*, *35*, 336–362, doi:10.1175/JPO-2690.1.

Di Lorenzo, E., et al. (2008), North Pacific Gyre Oscillation links ocean climate and ecosystem change, *Geophys. Res. Lett.*, *35*, L08607, doi:10.1029/2007GL032838.

Doney, S. C., S. Yeager, G. Danabasoglu, W. G. Large, and J. C. McWilliams (2007), Mechanisms governing interannual variability of upper-ocean temperature in a global ocean hindcast simulation, *J. Phys. Oceanogr.*, *37*, 1918–1938, doi:10.1175/JPO3089.1.

Durazo, R., and T. R. Baumgartner (2002), Evolution of oceanographic conditions off Baja California: 1997–1999, *Prog. Oceanogr.*, *54*, 7–31, doi:10.1016/S0079-6611(02)00041-1.

Durazo, R., G. Gaxiola-Castro, B. E. Lavaniegos, R. Castro-Valdez, J. Gomez-Valdes, and A. S. Mascarenhas Jr. (2005), Oceanographic conditions west of the Baja California coast 2002–2003: A weak El Niño and subarctic water enhancement, *Cienc. Mar.*, *31*, 537–552.

Emery, W. J., and K. Hamilton (1985), Atmospheric forcing of interannual variability in the northeast Pacific Ocean: Connections with El Niño, *J. Geophys. Res.*, *90*, 857–868, doi:10.1029/JC090iC01p00857.

Emery, W. J., and R. E. Thomson (2001), *Data Analysis Methods in Physical Oceanography*, 2nd ed., 638 pp., Elsevier Sci., Amsterdam.

Espinosa-Carreon, T. L., P. T. Strub, E. Beier, F. Ocampo-Torres, and G. Gaxiola-Castro (2004), Seasonal and interannual variability of satellite-derived chlorophyll pigment, surface height, and temperature off Baja California, *J. Geophys. Res.*, *109*, C03039, doi:10.1029/2003JC002105.

Freeland, H. J., G. Gatien, A. Huyer, and R. L. Smith (2003), Cold halocline in the northern California Current: An invasion of subarctic water, *Geophys. Res. Lett.*, *30*(3), 1141, doi:10.1029/2002GL016663.

Huyer, A. (2003), Preface to special section on enhanced subartic influence in the California Current, *Geophys. Res. Lett.*, *30*(15), 8019, doi:10.1029/2003GL017724.

Huyer, A., and R. L. Smith (1985), The Signature of El Niño off Oregon, 1982–1983, *J. Geophys. Res.*, *90*, 7133–7142.

Jacobs, G. A., H. E. Hurlburt, J. C. Kindle, E. J. Metzger, J. L. Mitchell, W. J. Teague, and A. J. Wallcraft (1994), Decade-scale trans-Pacific propagation and warming effects of an El Niño anomaly, *Nature*, *370*, 360–363, doi:10.1038/370360a0.

Jeronimo, G., and J. Gomez-Valdes (2006), Mean temperature and salinity along an isopycnal surface in the upper ocean off Baja California, *Cienc. Mar.*, *32*, 663–671.

Jeronimo, G., and J. Gomez-Valdes (2007), A subsurface warm-eddy off northern Baja California in July 2004, *Geophys. Res. Lett.*, *34*, L06610, doi:10.1029/2006GL028851.

Kara, A. B., P. A. Rochford, and H. E. Hurlburt (2000), An optimal definition for ocean mixed layer depth, *J. Geophys. Res.*, *105*, 16,803–16,821.

Le Traon, P. Y. (1990), A method for optimal analysis of fields with spatially variable mean, *J. Geophys. Res.*, *95*, 13,543–13,547, doi:10.1029/JC095iC08p13543.

Lynn, R. J. (1967), Seasonal variation of temperature and salinity at 10 meters in the California Current, *Calif. Coop. Fish. Invest. Rep.*, *11*, 157–186.

Lynn, R. J., and S. J. Bograd (2002), Dynamic evolution of the 1997–1999 El Niño–La Niña cycle in the southern California Current System, *Prog. Oceanogr.*, *54*, 59–75.

Lynn, R. J., and J. J. Simpson (1987), The California Current System: The seasonal variability of its physical characteristics, *J. Geophys. Res.*, *92*, 12,947–12,966, doi:10.1029/JC092iC12p12947.

Lynn, R. J., F. B. Schwing, and T. L. Hayward (1995), The effect of the 1991–1993 ENSO on the California Current System, *Calif. Coop. Fish. Invest. Rep.*, *36*, 57–71.

Mantua, N. J., and S. R. Hare (2002), The Pacific Decadal Oscillation, *J. Oceanogr.*, *58*, 35–44, doi:10.1023/A:1015820616384.

Mantua, N. J., S. R. Hare, Y. Zhang, J. M. Wallece, and R. C. Francis (1997), A Pacific interdecadal climate oscillation with impacts on salmon production, *Bull. Am. Meteorol. Soc.*, *78*, 1069–1079, doi:10.1175/1520-0477(1997)078<1069:APICOW>2.0.CO;2.

Marchesiello, P., J. C. McWilliams, and A. Shchepetkin (2003), Equilibrium structure and dynamics of the California Current, *J. Phys. Oceanogr.*, *33*, 753–783, doi:10.1175/1520-0485(2003)33<753:ESADOT>2.0.CO;2.

McPhaden, M. J. (1999), Genesis and evolution of the 1997–98 El Niño, *Science*, *283*, 950–954, doi:10.1126/science.283.5404.950.

Meinen, C. S., and M. J. McPhaden (2000), Observations of warm water volume changes in the equatorial Pacific and their relationship to El Niño

and La Niña, *J. Clim.*, *13*, 3551–3559, doi:10.1175/1520-0442(2000)013<3551:OOWWVC>2.0.CO;2.

Miller, A. J. (1996), Recent advances in California Current modeling: Decadal and interannual thermocline variations, *Calif. Coop. Fish. Invest. Rep.*, *37*, 69–79.

Miller, A. J., F. Chai, S. Chiba, J. R. Moisan, and D. J. Neilson (2004), Decadal-scale and ecosystem interactions in the North Pacific Ocean, *J. Oceanogr.*, *60*, 163–188, doi:10.1023/B:JOCE.0000038325.36306.95.

Norton, J. G., and D. R. McLain (1994), Diagnostic patterns of seasonal and interannual temperature variation off the west coast of the United States: Local and remote large-scale atmospheric forcing, *J. Geophys. Res.*, *99*, 16,019–16,030, doi:10.1029/94JC01170.

Pares-Sierra, A., and J. O'Brien (1989), The seasonal and interannual variability of the California Current System, *J. Geophys. Res.*, *94*, 3159–3180, doi:10.1029/JC094iC03p03159.

Perez-Brunius, P., M. Lopez, and J. Pineda (2006), Hydrographic conditions near the coast of northwestern Baja California: 1997–2004, *Cont. Shelf Res.*, *26*, 885–901, doi:10.1016/j.csr.2006.01.017.

Peterson, W. T., and F. B. Schwing (2003), A new regime in northeast Pacific ecosystems, *Geophys. Res. Lett.*, *30*(17), 1896, doi:10.1029/2003GL017528.

Peterson, W. T., et al. (2006), The state of the California Current, 2005–2006: Warm in the north, cool in the south, *Calif. Coop. Fish. Invest. Rep.*, *44*, 28–60.

Schneider, N., E. Di Lorenzo, and P. P. Niiler (2005), Salinity variations in the Southern California Current, *J. Phys. Oceanogr.*, *35*, 1421–1436, doi:10.1175/JPO2759.1.

Schwing, F. B., N. A. Bond, S. J. Bograd, T. Mitchell, M. A. Alexander, and N. Mantua (2006), Delayed coastal upwelling along the U.S. West Coast in 2005: A historical perspective, *Geophys. Res. Lett.*, *33*, L22S01, doi:10.1029/2006GL026911.

Soto-Mardones, L., A. Pares-Sierra, J. García, R. Durazo, and S. Hormazabal (2004), Analysis of the mesoscale structure in the IMECOCAL region (off Baja California) from hydrographic, ADCP and altimetry data, *Deep Sea Res., Part II*, *51*, 785–798.

Strub, P. T., and C. James (2000), Altimeter-derived variability of surface velocities in the California Current System: 2. Seasonal circulation and eddy statistics, *Deep Sea Res., Part II*, *47*, 831–870, doi:10.1016/S0967-0645(99)00129-0.

Sverdrup, H. U., M. W. Johnson, and R. H. Fleming (1942), *The Oceans: Their Physics, Chemistry, and General Biology*, 1087 pp., Prentice-Hall, Englewood Cliffs, N. J.

Taylor, J. R. (1997), *An Introduction to Error Analysis*, 2nd ed., 327 pp., Univ. Sci. Books, Sausalito, Calif.

Tomczak, M., and J. S. Godfrey (1994), *Regional Oceanography: An Introduction*, 422 pp., Elsevier Sci., Tarrytown, N. Y.

Wang, D.-P., and J. J. Walsh (1976), Objective analysis of the upwelling ecosystem off Baja California, *J. Mar. Res.*, *34*, 43–60.

White, W. B., C.-K. Tai, and J. DiMento (1990), Annual Rossby wave characteristics in the California Current region from the GEOSAT exact repeat mission, *J. Phys. Oceanogr.*, *20*, 1297–1311, doi:10.1175/1520-0485(1990)020<1297:ARWCIT>2.0.CO;2.

Zaytsev, O., R. Cervantes-Duarte, O. Montante, and A. Gallegos-Garcia (2003), Coastal upwelling activity on the Pacific shelf of the Baja California Peninsula, *J. Oceanogr.*, *59*, 489–502, doi:10.1023/A:1025544700632.

J. Gomez-Valdes, Physical Oceanography Department, CICESE, Km 107 Carretera Tijuana-Ensenada, Ensenada 22860, Mexico. (jgomez@cicese.mx)
G. Jeronimo, Facultad de Ciencias, UNAM, Sisal 97355, Mexico.